Exploring the influence of ionospheric O^+ outflow on magnetospheric dynamics: dependence on the source location

Yiqun Yu[1] and Aaron J. Ridley[2]

Received 16 October 2012; revised 21 November 2012; accepted 12 December 2012; published 30 April 2013.

[1] Heavy ions of ionospheric origin (O^+) play an important role in altering global magnetospheric dynamics. While the heavy ions mainly originate from the dayside cusp and the nightside auroral region, the impact of these heavy ions on magnetospheric dynamics has not been differentiated. Controversy also remains on the role of heavy ions on tail stability and their energization mechanism in the magnetosphere. Two global MHD simulations are carried out to investigate the influence of heavy ion outflow from different source regions on reconnection rates, tail stability, and ring current energization. The local reconnection rate at the subsolar point and the total dayside reconnection rate are reduced after the outflow begins, but the decrease is more significant when the outflow comes out of the cusp region. Furthermore, the magnetotail is more disturbed when heavy ions flow out of the dayside cusp region as opposed to the nightside auroral zone. This implies that the role of O^+ on tail stability is not definitively positive or negative; instead, the location of the source of heavy ions may be important in determining tail dynamics. Finally, the simulation reveals that the heavy ions originating from the dayside cusp region experience first adiabatic heating while traveling from the tail reconnection site toward the Earth and then further energization caused by flow braking near the outer boundary of the ring current.

Citation: Yu, Y., and A. J. Ridley (2013), Exploring the influence of ionospheric O^+ outflow on magnetospheric dynamics: dependence on the source location, *J. Geophys. Res. Space Physics*, *118*, 1711–1722, doi:10.1029/2012JA018411.

1. Introduction

[2] It is now generally accepted that ionospheric ions are a significant source of magnetospheric plasma and that the ionospheric plasma plays an important role in magnetospheric physics. The characteristics of outflowing ionospheric ions has been reviewed by *Yau and André* [1997] on the sources and energization mechanisms that drive the ions upward to high altitudes and then into the magnetosphere. The various characteristics of the ionospheric heavy ions (i.e., O^+) inside the magnetosphere has also been largely carried out [e.g., *Nosé et al*., 2000a; *Nosé et al*., 2005; *Nosé et al*., 2009; *Kistler et al*., 2005; *Kistler et al*., 2006; *Kistler et al*., 2010; *Ebihara et al*., 2006; *Fok et al*., 2006]. A common scenario from these studies is that the ionosphere-origin heavy ions inside the magnetosphere undergo dramatic enhancements in both number and energy densities during highly disturbed time, possibly exceeding that of protons. For the ionospheric plasma transport and energization, the fate of the ionospheric plasma, and the impact on the coupled magnetosphere/ionosphere system, readers can refer to a tutorial work by *Lotko* [2007].

1.1. Source Location

[3] The ionospheric heavy ions can flow out of various ionosphere regions, among which two major source locations receive considerable attentions in the past. One source is the cleft ion fountain [*Lockwood et al*., 1985], which is a persistent reservoir for providing upwelling ions but is not a dominant source for the ionospheric outflow into the magnetosphere during solar minimum quiet time [*Peterson et al*., 2006]. Such cusp-originated O^+ ions are transported across the polar cap into the lob region and finally are deposited into the plasma sheet and the ring current through tail reconnection [*Elliott et al*., 2007; *Kistler et al*., 2010; *Liao et al*., 2010]. Another pathway for the ionospheric outflow into the plasma sheet is directly out of the nocturnal auroral oval, which generates energetic and large fluxes of O^+ during storm times [*Tung et al*., 2001]. The auroral O^+ flows along magnetic field lines into the magnetosphere, providing rapid feeding to the plasma sheet and ring current [*Daglis and Axford*, 1996].

[4] Since the ionospheric heavy ions originate from various source regions, many researchers have numerically traced ionospheric outflow starting from different source regions through test particle techniques [e.g., *Moore et al*., 2005; *Peroomian et al*., 2006; *Winglee*, 2003; *Delcourt et al*., 1989] or through fluid MHD simulations [e.g.,

[1]Space Science and Application, ISR-1, Los Alamos National Laboratory, Los Alamos, New Mexico, USA.
[2]Department of Atmospheric, Oceanic and Space Sciences, University of Michigan, Ann Arbor, Michigan, USA.

Corresponding author: Yiqun Yu, Space Science and Application, ISR-1, Los Alamos National Laboratory, Los Alamos, NM 87545, USA. (yiqun@lanl.gov)

2169-9380/13/2012JA018411

Wiltberger et al., 2010; *Garcia et al*., 2010; Brambles et al., 2010]. They found that the ionospheric ions could dominate the ring current during geomagnetically active time and that, after the ionospheric outflow, the changes within the magnetosphere–ionosphere system, such as the CPCP index, the ring current intensity, plasma sheet properties, and the tail geometry, appear to be associated with the outflow intensity, and the heavy ions out of different source regions can populate in different inner regions and experience different processes along the way into the inner magnetosphere.

1.2. Tail Dynamics

[5] One debate within the magnetospheric community regards the role of ionospheric heavy ions in a substorm. *Baker et al*. [1982] first suggested that the O^+ increases the growth rate of the linear ion tearing mode instability, thereby leading to a faster initialization of substorms. *Kistler et al*. [2006] could not find the expected role of O^+ in decreasing the threshold of substorm onset. *Lennartsson et al*. [1993] suggested that O^+ ions do not have geomagnetic feedback in the magnetotail after they studied the correlation between the average O^+ abundance and different geomagnetic indices. *Nosé et al*. [2009] found a negative correlation or no correlation between the long-term plasma sheet ion composition and substorm occurrence, so they suggested that the O^+ ions in the plasma sheet may prevent occurrence of substorms, in contrast with the O^+ triggering substorm model. While the last two studies both utilized long-time averaged quantities of O^+ observations to examine the geomagnetic feedback of O^+ ions, *Daglis and Sarris* [1998] disputed the feasibility of using averaged quantities by raising the question of temporal scales. They argued that as a substorm is triggered on a shorter time scale, the long-term averaged quantities could not reflect the transient participation of the heavy ions in the substorm so that the possible role of O^+ in the substorm would not be excluded. However, none of the above arguments relate the substorm stability with the heavy ions originated from different ionospheric source regions; this study will investigate such relationship by separately initializing the ionospheric outflow from the dayside cusp region and the nightside auroral region.

1.3. Energization

[6] Another fundamental question associated with the energization of O^+ inside the magnetosphere is whether the storm-enhanced O^+ energy density is a result of (1) the direct ejection of energetic plasma out of the ionosphere [*Sheldon et al*., 1998]; (2) localized energization of preexisting O^+ in the plasma sheet [*Nosé et al*., 2000a; *Delcourt*, 2002; *Fok et al*., 2006; *Nosé et al*., 2010]; or (3) the capture and subsequent acceleration of in-flight/in-transit O^+ in the lobe region [*Peterson et al*., 2009].

[7] *Sheldon et al*. [1998] suggested that the acceleration process of the energetic oxygen beams inside the plasma sheet is associated with parallel electric fields near the ionosphere, such that the O^+ arrives in the plasma sheet already energized. In contrast to this, other studies advocate a localized energization in the plasma sheet. For example, *Fok et al*. [2006] argued that the ionospheric cusp-origin ions with energy less than 1 keV would take hours to arrive in the plasma sheet and become energized and thus could not explain the prompt increase in the energy density. They simulated an idealized substorm by using the LFM MHD model [*Lyon et al*., 2004] and concluded that the O^+ prompt enhancement is a result of nonadiabatic energization of the preexisting O^+ in the plasma sheet when dipolarization takes place. *Delcourt* [2002] suggested that the preexisting O^+ in the plasma sheet is accelerated by inductive electric fields in the inner magnetosphere while being moved earthward. *Nosé et al*. [2000b] showed observationally that the O^+ energy density enhancement is caused by local magnetic field dipolarization in the near-Earth plasma sheet region. *Nosé et al*. [2010] proposed that the O^+ -rich ring current is generated from the local and nonadiabatic acceleration of the preexisting thermal O^+ in the outer plasma sheet by magnetic fluctuations.

[8] The third proposal for the enhanced O^+ energy density in the inner magnetosphere is through tail reconnection, which captures the ions in the lobes and accelerates them. *Peterson et al*. [2009] analyzed the relative magnitude of the O^+ population in transit between the ionosphere and the ring current in the quiet time before geomagnetic storms and suggested that the dynamics during the storm alters the O^+ pathways from the ionosphere to the ring current and that the preexisting in-transit O^+ population is captured by the magnetic field into the ring current during the magnetic storm. *Peroomian et al*. [2006] simulated dayside O^+ outflow using test particle tracing through an MHD model and found that the O^+ number and energy density in the plasma sheet and ring current respond almost instantly to an interplanetary shock. They suggested that the rapid enhancement is caused by the acceleration of ions already en route to the plasma sheet.

[9] Again, all these debates regarding the O^+ energization in the inner magnetosphere overlook one important fact that may influence their conclusions, that is, the source location of the ionospheric outflow. This work will explore the role of ionospheric outflow from different source locations in altering magnetospheric dynamics and discuss how the ionospheric O^+ ions, appearing in the inner magnetosphere, undergo energization.

1.4. Methods for Outflow Specification

[10] A variety of outflow configurations in MHD simulations have been used to initialize the ionospheric outflow. Recently, a popular method in studying the ionospheric mass outflow in MHD simulations has been to apply an empirically driven formula onto the polar region [e.g., *Gagne*, 2005; *Brambles et al*., 2010; *Moore et al*., 2010]. In these studies, the Strangeway formula [*Strangeway et al*., 2005] was applied to specify the O^+ ion number flux at the inner boundary of a global magnetospheric MHD code. The formula was derived from a large number of FAST observations of dayside cusp O^+ upwelling flux at 4000 km altitude based on downward directed Poynting flux or precipitating electron density.

[11] A different method of incorporating the ionospheric outflow into a MHD model is to couple with a self-consistent ionospheric outflow model. For example, *Glocer et al*. [2009b] implemented a first-principle polar wind outflow model (PWOM) into the space weather modeling framework (SWMF) [*Tóth et al*., 2005] at the University of Michigan, which self-consistently represents the physics in the driving mechanisms of the upwelling and outflowing as well as the feedback from the global magnetosphere.

[12] Different from both of the above outflow specification methods, *Garcia et al*. [2010] used constant outflow conditions over a nightside auroral region to intentionally examine the single effect of the nightside outflow intensity. This is the method that will be employed in this study.

[13] As stated above, the dependence on the source location has not yet been fully explored while determining the role of ionospheric heavy ions in changing magnetospheric dynamics, including the tail stability and the ring current energization. Therefore, this work will focus on the effect of ionospheric heavy ions emanated from two different source regions (i.e., dayside cusp outflow and nightside aurora outflow) on the dayside reconnection rate and tail stability and will discuss the mechanisms of the energization of heavy ions in the inner magnetosphere.

2. Methodology

[14] The global multifluid MHD model Block-Adaptive Tree Solar-wind Roe Upwind Scheme (BATS-R-US) is used in this study. The multifluid code solves MHD equations for two ion fluids (i.e., H^+ and O^+) with their individual mass, momentum, and energy equations [*Glocer et al*., 2009b]. The physical domain covered by this MHD model extends from 32 R_e on the dayside to 224 R_e on the nightside in the Sun–Earth direction and $\pm$ 128 R_e in the other two directions. The state of the magnetosphere is controlled by solar wind conditions at the upstream outer boundary at 32 R_e and ionosphere conditions at the inner boundary at 2.5 R_e. The solar wind conditions at the upstream boundary can be obtained either from other model output [*Ridley et al*., 2006] or from real observations such as ACE or wind measurements [e.g., *Yu and Ridley*, 2008] or even from user-designed conditions [e.g., *Yu and Ridley*, 2009a, 2009b]. Other outer boundaries use zero gradient in the solar wind plasma parameters since these boundaries are too far from the Earth to influence the near-Earth dynamics. The inner boundary of the MHD code is a spherical shell at 2.5 R_e and requires the specification of density, velocity, and temperature for both ion fluids. These parameters on the inner boundary of the MHD model are essentially the controlling factors in this study, as they describe the conditions of the ionospheric source region.

[15] The inner boundary is partially controlled by the ionospheric electrodynamics model [*Ridley et al*., 2004] in such a way that the field-aligned current computed near the inner boundary of the MHD code is mapped down to the ionospheric model to obtain the electric potential. This potential is then mapped back out to the inner boundary of the MHD code to compute the convection velocity across the field lines. No parallel electric potential drop is allowed in the region between the ionosphere and the inner boundary of the MHD model. The conductivity used in the ionospheric model is not uniform but structured, depending on the mapped field-aligned currents. The conductance used in the ionospheric solver includes solar-generated conductance, nightside conductance, and auroral zone conductance (details about the influence of the ionospheric conductance on the magnetosphere can be found in the study by *Ridley et al*. [2004]). The number density and temperature of each species are specified in a given way to produce field-aligned outflow and is described in section 2.2.

[16] These coupled modules have been validated by comparisons against a wide variety of observations, such as ground-based magnetic field perturbations [*Yu and Ridley*, 2008; *Yu et al*., 2010], magnetic and plasma observations from CHAMP and DMSP satellite [*Wang et al*., 2008], and magnetospheric magnetic field and plasma observed by geosynchronous satellites [*Welling and Ridley*, 2010].

2.1. Resolution and Resistivity

[17] To control the diffusion in the reconnection site in an MHD code, the resolution needs to be increased to the point in which the numerical resistivity is lower than the required physical resistivity. Once this is achieved, resistivity is added at a realistic value, and the reconnection rate is controlled physically [*Borovsky et al*., 2008].

[18] In this study, a 1/16 R_e grid resolution is employed in the area of interest (i.e., from X: [6, 16], Y: [-12, 12], Z: [-12, 12] R_e) where the reconnection occurs on the dayside magnetopause boundary, and a 1/8 R_e grid resolution is applied around the inner body. A coarser resolution of 1/4 R_e is imposed in the tail region because it is impossible to use a small fixed high-resolution region in the tail due to the mobility of the tail X-line, and a large number of high-resolution grid cells take significantly more computational time. It should be noted that a coarser resolution introduces more numerical resistivity, but its exact effect on reconnection compared to the physical resistivity is unknown [*Ridley et al*., 2010]. It may create unbalanced reconnection between dayside and nightside at times, but within the simulations described below, the magnetosphere seems to reach a roughly steady state quickly, indicating that the different types of resistivity in the dayside and tail reconnection sites seem not to have significantly different effects.

[19] The required high resistivity within the reconnection site is obtained through a current-dependent anomalous resistivity (η) that is applied in the global domain:

$$\eta = \eta_0 + min\left\{\eta_{max}, max\left[0.0, \eta_{a0}\left(\frac{|J|}{J_C} - 1\right)\right]\right\} \qquad (1)$$

where constants η_0, η_{max}, η_{a0}, and J_c are chosen to be $1.0 \times 10^9\ m^2/s$, $2.0 \times 10^{10}\ m^2/s$, $2.0 \times 10^9\ m^2/s$, and $1.0 \times 10^{-9}\ A/m^2$, respectively. From equation (1), the anomalous resistivity η is large in areas where the current density exceeds the threshold J_c, while it is small in the rest of the simulation domain. Note that this formula does not exclude regions such as the near-Earth boundary where the field-aligned currents may be large.

2.2. Setup for Outflow Simulations

[20] To simulate the ionospheric outflow, boundary conditions are imposed at the inner boundary of the MHD model. Instead of applying the Strangeway formula or the self-consistent outflow model, a simple constant area-confined outflow is specified, similar to that of *Garcia et al*. [2010]. Two simulations are carried out to examine the effect of outflow originating from different source regions (i.e., cusp region and nightside auroral region) on the magnetospheric dynamics. For the simulation that investigates the cusp outflow (cusp outflow simulation), the ionospheric plasma flows out from a wedge-shape region at the inner boundary from 65° to 85° magnetic latitude (i.e., 74.5° – 86.8° magnetic

latitude at the ionosphere altitude if mapped down along dipole magnetic field lines) and from 11 to 13 magnetic local time (MLT). The simulation with nightside auroral outflow (nightside auroral outflow simulation) uses a wedge-shape source region at the inner boundary on the nightside from 23 to 01 MLT across midnight and from 55° to 75° magnetic latitudes (i.e., 68.7° – 80.6° at the ionosphere altitude). The necessary parameters in these source regions are $N_{O^+} = 20\,cm^{-3}$, $V_{O^+||} = 50$ km/s, $T_{O^+} = 1,000,000$ K, $N_{H^+} = 10$ cm^{-3}, $V_{H^+||} = 0$ km/s, and $T_{H^+} = 100,000$ K. The rest of the spherical boundary is specified by $N_{O^+} = 0.01$ cm^{-3}, $V_{O^+||} = 0$ km/s, $T_{O^+} = 25,000$ K, $N_{H^+} = 28$ cm^{-3}, $V_{O^+||} = 0$ km/s, and $T_{H^+} = 25,000$ K. Here, "||" denotes the outward direction along the magnetic field lines. H^+ is forced to have little outflow (V_{H^+} is zero, but numerical diffusion still allows limited outflow). For the dayside cusp and nightside auroral outflow simulations, fluence rates of O^+ over the entire northern hemisphere at 3.5 R_e are about 1.65×10^{25} ions/s and 2.732×10^{25} ions/s, respectively, which fall in the range of observed statistics [*Cully et al.*, 2003]. Therefore, even though these experiments are highly idealized, they do mimic reality in their global outflow rates. Further note that the specification of one single source region (without the other one) in either simulation is particularly designed for the study of the role of the source region, even though in reality, both regions can simultaneously provide ionospheric heavy ions to the magnetosphere, while the ratio of the two may vary.

[21] The ionospheric plasma under the above-specified conditions begins to flow out of these source regions when the system is under a steady state, which was obtained by driving the system with constant solar wind conditions (i.e., $N_{sw} = 5$ cm^{-3}, IMF $B_z = -5$ nT, $B_x = B_y = 0$, and $V_x =$ 400 km/s) and zero-outflow inner boundary conditions for 3 hours. Simulation results shown later will all start from 02:00, 1 hour before the outflow begins. The solar wind conditions remain the same throughout the entire outflow simulation time.

3. Simulation Results

[22] The temporal evolution of the heavy ions flowing out from the ionospheric cusp region to the plasma sheet in the X-Z plane is illustrated in Figure 1a. Color represents the number density of O^+ ions on a log scale and the lines represent the in-plane magnetic field lines. Originating from a restricted region in the ionosphere, the majority of the plasma out of the cusp region travels first upward along the magnetic field and then tailward across the high-altitude polar cap aided by the tailward streaming solar wind. The O^+ streams into the lobe region and is captured by the tail reconnection which ejects it earthward. The heavy ions then travel preferentially along the magnetic field lines toward higher latitude in both hemispheres, forming a bifurcated pattern along the plasma sheet boundary in the X-Z plane. It finally diffuses into the inner magnetosphere.

[23] Figure 1b shows the flow path of heavy ions out of the nightside auroral region. Most of the ionospheric O^+ flows into the inner magnetosphere along nightside closed field lines without going through the tail reconnection site. Some ionospheric O^+ on open field lines stream down to the tail along the plasma sheet boundary and participate in the tail reconnection but at a much lower level than in the cusp outflow simulation. Note that even though the primary outflow occurs on the nightside, the upwelling along the field lines is accompanied by perpendicular diffusion so that a small amount of outflow ions escape into the dayside magnetosphere.

3.1. Tail Dynamics, CPCP Index, and Magnetopause Motion

[24] Figure 2 illustrates the cross polar cap potential (CPCP) index, the tail X-line position on the Sun–Earth line, and the earthward ejection speed in the reference frame of the tail reconnection site for the cusp outflow simulation (solid) and nightside auroral outflow simulation (dash).

[25] Before the outflow occurs at 03:00, both simulations are under the same solar wind driving conditions, therefore, the CPCPs are the same for the two simulations. After the outflow starts at 03:00 in different ionospheric source regions, the potentials in both simulations are reduced followed by a small recovery. The reduction in CPCP index caused by the mass outflow is consistent with earlier studies [e.g., *Brambles et al.*, 2010; *Glocer et al.*, 2009a; *Winglee et al.*, 2002], but it differs in the magnitude between these two simulations. The CPCP in the cusp outflow simulation decreases more, indicating that the influence of cusp O^+ outflow is more profound, although it has less outflow fluence due to a smaller outflow area. The CPCP recovers to a slightly higher level in the cusp outflow simulation.

[26] The tail dynamics in the two outflow configurations are striking different after the outflow, as seen in Figure 2b. The magnetotail appears quiet and steady with the X-line staying around -20 R_e in the nightside auroral outflow simulation, while the tail in the cusp outflow simulation experiences dramatic changes. In the latter case, the X-line location shifts quickly from the original position (near -20 R_e) to as far as -50 R_e down tail, followed by an earthward dipolarization half an hour later (around 04:35) (this dipolarization can also be observed in the enhancement of the magnetic field at the same time in Figure 6) and a final relaxation to a relatively steady position at -44 R_e. The fast tailward shift (between 03:45 and 04:00) of the tail is associated with a plasmamoid formed after the O^+ reaches the plasma sheet.

[27] Figure 3 shows the formation of the plasmamoid tailward of the X-line. The plasmamoid is circled by the red line or the zero B_z contour line. This plasmamoid is distorted and east-west asymmetric, with the west side traveling earthward. Subsequently, this part of the plasmamoid detaches from its original island and "dissolves" into the closed field region (at 03:55), expanding the X-line to be more tailward (04:00).

[28] The speed of earthward plasma convection out of the tail reconnection site is seen to be significantly smaller compared to when there was no outflow as shown in Figure 2c, which is a signature of a reduced reconnection rate. This reduction is also observed in the nightside auroral outflow simulation, even though the tail stays steady: the earthward ejection speed drops by a factor of about 4 with the nightside outflow; however, it is less than the reduction in the cusp outflow simulation where the speed is reduced by roughly a factor of 8.

[29] The dayside is also affected by the outflow as evidenced by the motion of the magnetopause. *Brambles et al.* [2010] found both outward and inward motion of the magnetopause after the dayside magnetosphere cavity was populated with new heavy plasma from different outflow

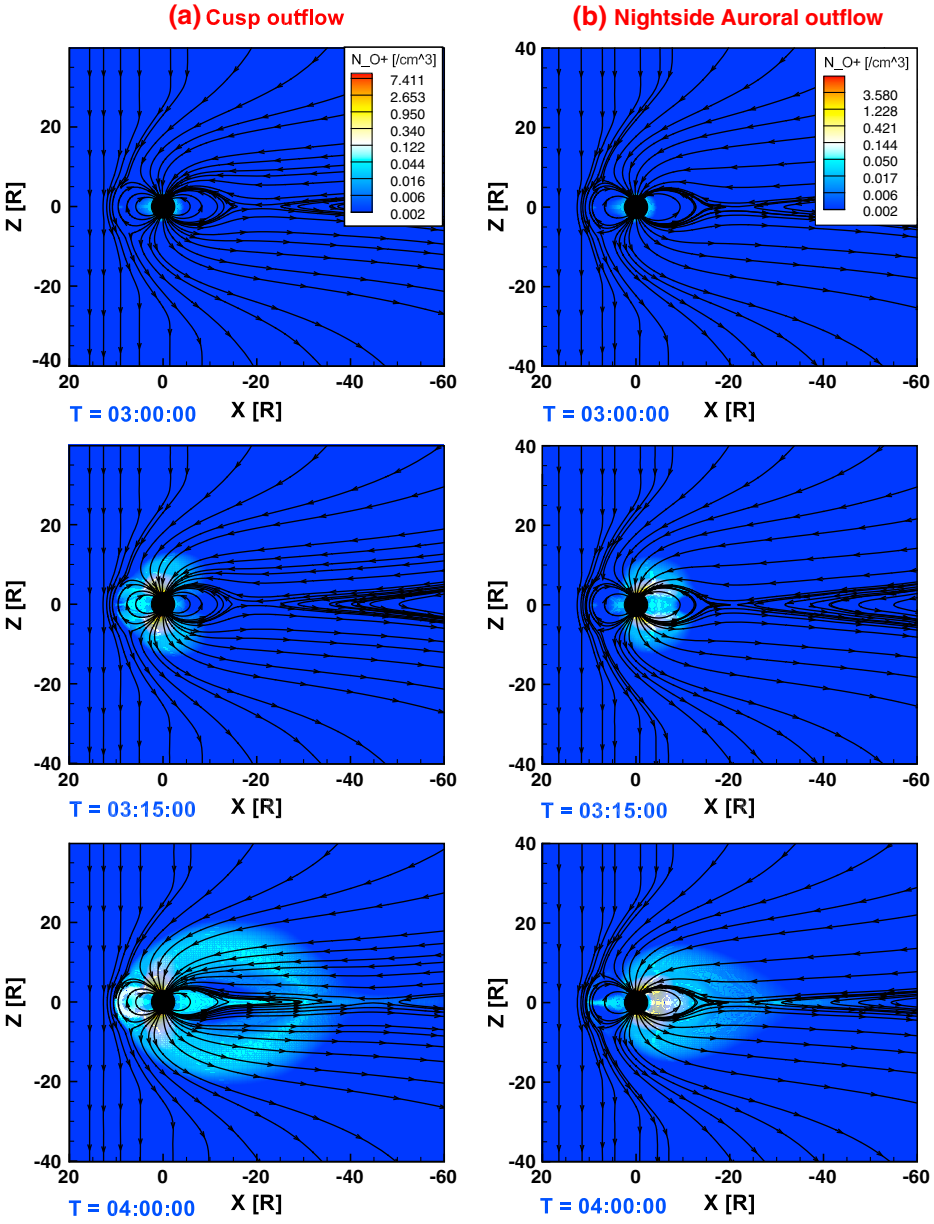

Figure 1. The evolution of ionospheric O^+ outflow from the dayside cusp region (column (a)) and nightside auroral region (column (b)) starting at 03:00. Color represents the number density of O^+ and the lines are the in-plane magnetic field lines.

regions with different thermal conditions. In this study, while the nightside auroral outflow simulation barely shows any motion of the magnetopause, the cusp outflow simulation indicates that after the initialization of outflow in the cusp region, the magnetopause travels toward the Earth as far as 0.4 R_e within 2 hours (Figure 4a), approximately equal to a speed of 355 m/s. It then moves outward slightly. The inward motion of the magnetopause is likely associated with the decrease of the magnetic field magnitude inside the magnetopause, since the magnetopause occurs where the solar wind ram pressure equals the magnetic pressure of the magnetospheric field plus the thermal pressure (usually, this component is neglected due to its small magnitude). The solar wind conditions in this study remain constant, so any change in the magnetopause position would have to be caused by the change in the magnetospheric processes. The total pressure at (9, 0, 0) R_e, which is just inside the magnetopause, as illustrated in Figure 4b, decreased until 4:45 when the total pressure slightly recovered, which is consistent with the outward movement of the magnetopause. While the magnetic pressure stopped decreasing after this time, the thermal pressure continued increasing due to the arrival of hot ions, resulting in an enhanced magnetospheric pressure and hence an outward motion of the magnetopause.

[30] The possible reason for a decreased magnetic field near the dayside magnetopause is that two magnetospheric current systems are strengthened: (1) the tail current was strengthened due to the extended thinner magnetotail, and (2) a small partial ring current was formed. These two current systems induce southward magnetic fields at the dayside

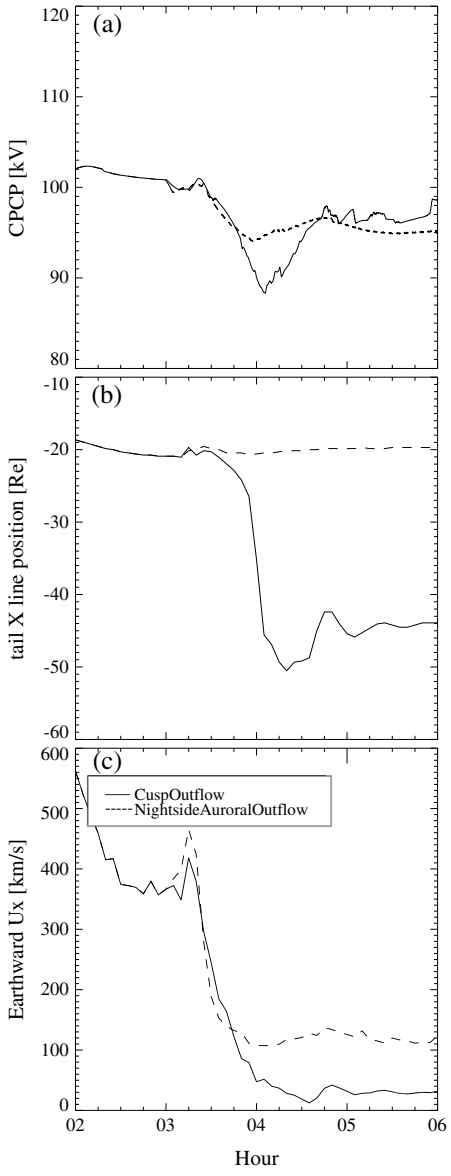

Figure 2. (a) The CPCP index, (b) tail X-line position, and (c) earthward ejection speed on the earthside of X-line in the reference frame of tail reconnection site for the cusp outflow simulation (solid) and nightside auroral outflow simulation (dashed). The outflow starts at 03:00.

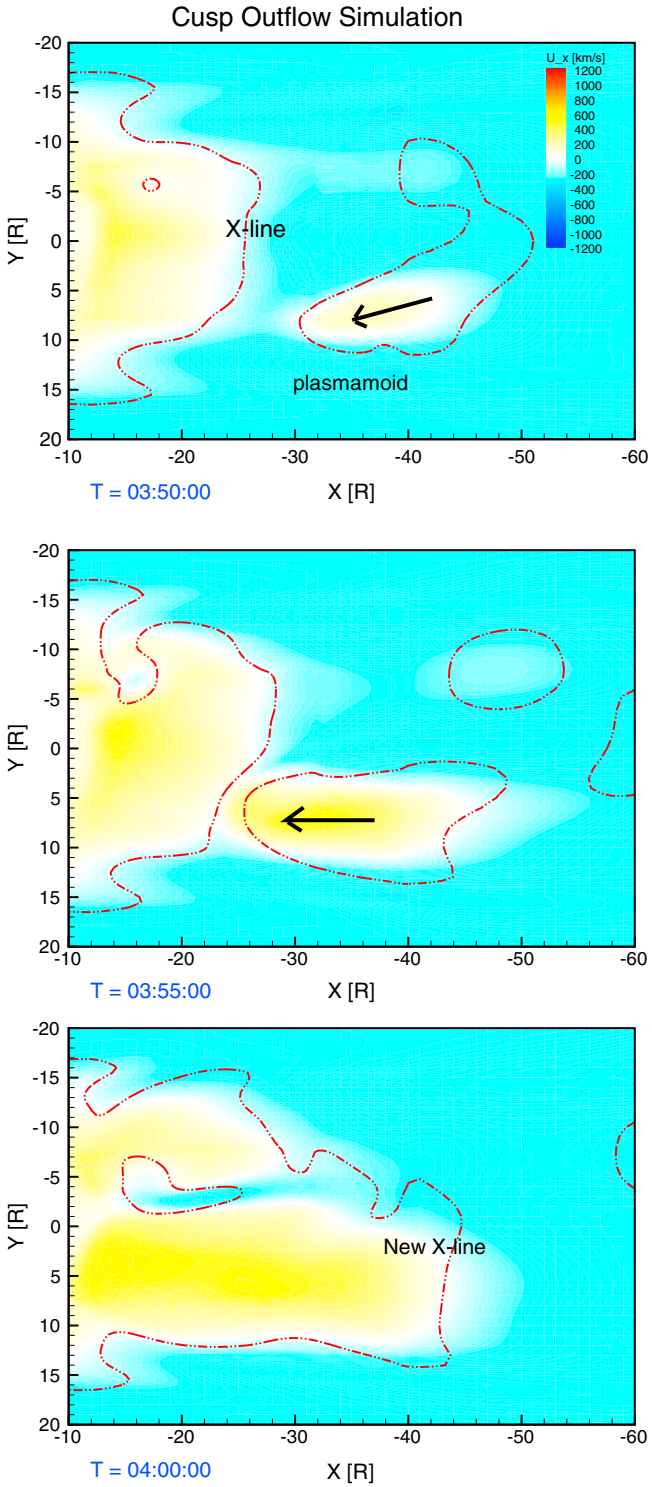

Figure 3. The formation of a plasmamoid tailward of the X-line after the mass loading on the plasma sheet in the cusp outflow simulation. Color represents the velocity in X direction: yellow indicates Earthward convection and blue means tailward convection. The red dash-dot line indicates the zero $\boldsymbol{B_z}$ contour.

magnetosphere, partially counteracting the intrinsic northward geomagnetic field, causing the net magnetic field to decrease and the magnetopause to shift inward.

[31] Figure 4c shows the southward magnetic fields induced by the tail current (dash) and the ring current (dash-dot) on the dayside Sun–Earth line at 9 R_e. The magnetic field is calculated by the Biot–Savart integral over 3D volumes of (X:[-14,-35] R_e, Y:[-14,14] R_e, Z: [-0.5,0.5] R_e) for the tail current and (X:[-5,-10] R_e, Y:[-14,14] R_e, Z: [-2,2] R_e) for the ring current. The induced magnetic field from the tail current shows a small increase, but the contribution from the ring current begins to increase after the tail reconfiguration and eventually contributes a significantly larger perturbation than the tail current. It should be noted that the induced magnetic fields may be larger than the above estimated values, since the integral volume chosen here does not comprehensively cover the ring current region which is partial ring-shape around the Earth rather than a rectangular box as confined in this estimation. As shown in Figure 4b, the real reduction in

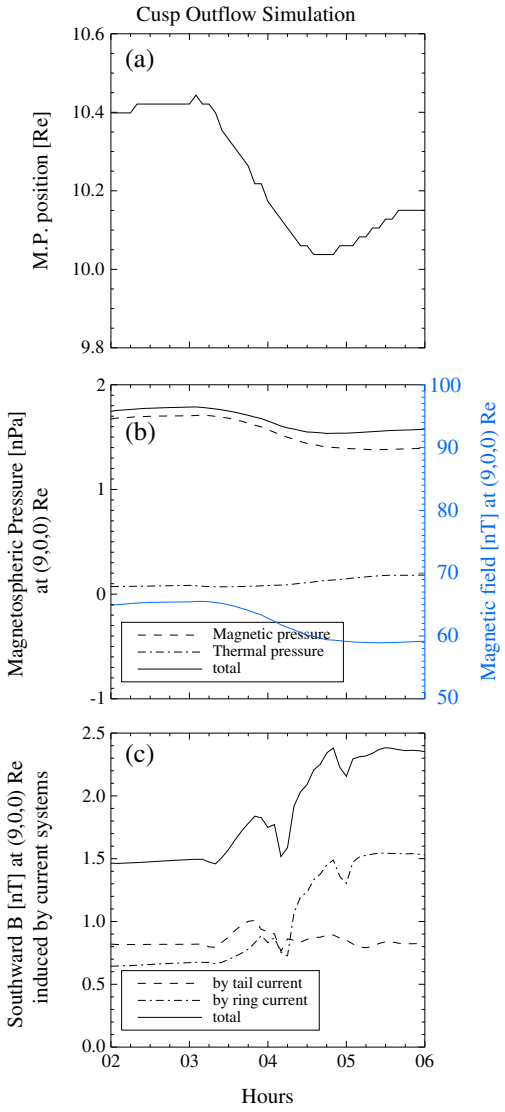

Figure 4. In the cusp outflow simulation, (a) the position of the dayside subsolar magnetopause as a function of time. (b) the magnetic pressure (dash) and thermal pressure (dash-dot) inside the subsolar magnetopause. (c) Induced magnetic fields at position of (9, 0, 0) $\boldsymbol{R_e}$ on the dayside Sun–Earth line calculated by the Biot–Savart integral from ring current source (dash-dot) and tail current (dash) source in a box of (X:[-5,-10] $\boldsymbol{R_e}$, Y:[-14,14] $\boldsymbol{R_e}$, Z: [-2,2] $\boldsymbol{R_e}$) and (X:[-14,-35] $\boldsymbol{R_e}$, Y:[-14,14] $\boldsymbol{R_e}$, Z: [-0.5,0.5] $\boldsymbol{R_e}$) respectively.

the magnetic field is much larger than this calculated induced magnetic field. Therefore, the calculation here is only an estimate, providing insight into the possible tendency of the current systems in changing the magnetospheric field topology.

3.2. Reconnection Rate

[32] Dayside reconnection plays an important role in transferring solar wind energy into the magnetosphere. The local reconnection rate is typically measured by an effective electric field [*Hu et al.*, 2009]. This effective electric field is then multiplied by an effective length of the reconnection merging line, resulting in a reconnection voltage, representing the total dayside (global) reconnection rate [*Hu et al.*, 2009]. The local rate at the subsolar point describes the local strength of magnetic reconnection and can help reveal the localized impact of heavy ions on the subsolar point. The global rate can indicate how the heavy ions disturb the global state. These two rates are therefore employed to investigate the impact of the heavy ions on the magnetosphere.

[33] The local reconnection rate is measured at the subsolar magnetopause using the scaling law derived by *Cassak and Shay*, [2007]:

$$CS = 2(B_1B_2)^{3/2}(\mu_0\rho_1B_2 + \mu_0\rho_2B_1)^{-1/2}(B_1 + B_2)^{-1/2} \quad (2)$$

where B and ρ are the magnetic field and total mass density ($\rho = M_{H^+}N_{H^+} + M_{O^+}N_{O^+}$), respectively; the indices "1" and "2" denote the magnetosheath and magnetospheric sides, respectively; and μ_0 is the vacuum permeability. This CS scaling law essentially expresses the reconnection rate in terms of local plasma properties near the reconnection site and has been verified by *Borovsky et al.* [2008] using the common expression of reconnection rate (i.e., ηJ, where η is the resistivity and J is the current density at the reconnection site). They concluded that the CS formula can very well describe the reconnection rate near the dayside magnetopause under southward IMF conditions. In this study, the parameters needed in the formula are taken along the Sun–Earth line at positions where the magnetic field profile starts to steepen toward the magnetopause on both the magnetosheath and magnetospheric sides. The motion of the magnetopause is therefore implicitly included.

[34] The local subsolar reconnection rates for both the cusp outflow and nightside auroral outflow simulations are illustrated in Figure 5. Both reconnection rates are reduced after the ionospheric O^+ ions enter the magnetosphere, but the differences between the two rates lie both in the time when the rate reaches its minimum value and the magnitude of the depression. In the cusp outflow simulation, there is a dip right after 03:00 which is followed by a quick rebound between 03:15 and 04:00, before a large depression. Although the flux rate of the ionospheric O^+ out of the cusp region (cusp outflow simulation) is smaller than that in the nightside auroral outflow simulation due to its smaller outflow area, the reconnection rate is nevertheless depressed more (down to $7.7mV/m$ in the cusp outflow simulation versus $8.0mV/m$ in the nightside auroral outflow simulation). Furthermore, the depression in the cusp outflow simulation lasts longer before the reconnection rate recovers.

[35] Figure 5b shows the magnetic field (blue) and mass density (black) on the magnetospheric side of the subsolar magnetopause in the cusp outflow simulation. The total mass density just inside the nose of the magnetopause is enhanced immediately after the outflow, consistent with the quick dip shown in the reconnection rate. However, the prominent influence from the mass density occurs after 04:00 when the total mass density is enhanced, which significantly weakens the reconnection rate. O^+ ions constitute a small percentage in the total mass density so that the increase in H^+ density plays the predominant role in decreasing the reconnection rate. The variation in the H^+ mass density is associated with the motion of a plume connecting the inner magnetosphere with the magnetopause, which

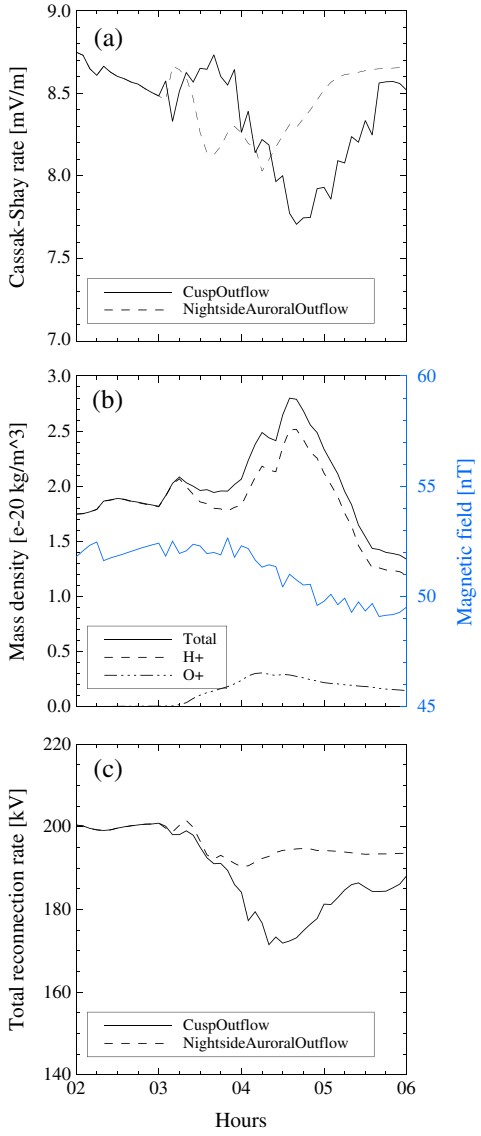

Figure 5. (a) Local reconnection rate for the cusp outflow simulation (solid) and nightside auroral outflow simulation (dashed). (b) The mass density of two fluids and magnetic field taken for the CS formula for the cusp outflow simulation. (c) The total dayside reconnection rate for the cusp outflow simulation (solid) and nightside auroral outflow simulation (dashed).

shifts westward across the nose of the magnetopause after the initiation of the ionospheric outflow (not shown). However, the mass density change at the magnetopause is not the sole factor of the reduction in the reconnection rate. The magnetic field is gradually attenuated after 04:00 and reaches a relatively steady state after 05:00. Both the diminished magnetic field and the enhanced mass density near the subsolar magnetopause are responsible for the decreased subsolar reconnection rate.

[36] Unlike these dynamical changes of the magnetospheric plasma and field in the cusp outflow simulation, the magnetospheric field near the subsolar point in the nightside auroral outflow simulation showed little change (not shown). The mass density increased and then declined, with the changes predominantly from H^+ ions, implying that the changes in the H^+ mass density were mostly responsible for altering the reconnection rate in the nightside auroral outflow simulation.

[37] The total dayside reconnection rate is represented by the potential drop along the merging line on the dayside magnetopause, as explained above. For an idealized simulation with zero tilt angle of the dipole magnetic field, the merging line can be easily determined by selecting the minimum magnetic field magnitude across the magnetopause in the equatorial plane. Under purely southward IMF conditions, the potential along the merging line displays a sine-shape profile with the extrema approximately on the dawn and dusk magnetopause [*Hu et al.*, 2009]. Therefore, calculating the electric potential along the entire merging line is not necessary, instead, knowing the electric potentials on the dawn and dusk magnetopause is sufficient to obtain the total reconnection rate (i.e., the difference between the two extrema), significantly simplifying the calculation due to the numerical effort that would be needed in searching for the merging line.

[38] The electric potential on the dawn and dusk magnetopause is obtained by integrating the electric field radially from the inner boundary ($2.5R_e$) to the dawn/dusk magnetopause boundary in the equatorial plane. The electric potential drop along the merging line (or the potential difference between the dusk and dawn potentials as simplified in this study) is almost equal to the rate of change of magnetic flux that is reconnected through the magnetopause boundary. The proof is shown in Appendix A.

[39] Figure 5c shows the total dayside reconnection rate for the cusp outflow case (solid line) and nightside auroral outflow case (dashed line). The total reconnection rate with the cusp outflow is significantly reduced after the outflow at 03:00, reaching a minimum value at 04:30 and recovering after two and a half hours, while in the nightside auroral outflow simulation, the rate shows little change, although it is somewhat decreased. A smaller potential drop means that, in a unit of time, less net magnetic flux is reconnected through the dayside magnetopause boundary and that less magnetic energy is converted into plasma kinetic energy that transmits down into the ionosphere. This decreased amount of transmitted energy into the ionosphere is reflected in the decreased CPCP index (see Figure 2a).

[40] For the cusp outflow case, the smaller amount of reconnected magnetic flux is associated with two factors, which have already been discussed: (a) the magnetic field inside the magnetopause is decreased due to the growth of the partial ring current on the nightside and tail current, and (b) the magnetosphere is smaller as the dayside magnetopause moves inward while the dawn/dusk magnetopause generally stays still, leading to a smaller reconnection area or separatrix line. After 04:30 when the magnetopause returns sunward and the magnetic field inside the magnetopause remains at a nearly constant value, the reconnection rate starts to recover.

[41] No evidence of motion of the magnetopause or decrease in the magnetic field is observed in the nightside auroral outflow simulation, indicating that the total magnetic flux reconnected on the dayside magnetopause boundary should change little, i.e., the total dayside reconnection rate should change little, which is exactly the situation shown in Figure 5c.

4. Discussion

4.1. Effect of Plasma Diffusion on the Boundary

[42] Due to numerical diffusion across grid cells in the presence of a large pressure gradient, the designated 20° outflow area is broadened so that part of O^+ ion source also diffuses across the magnetic field to lower latitudes and enters the dayside magnetospheric cavity (see Figure 1a). This portion of O^+ ions is comparable to the O^+ density in the plasma sheet. However, these diffused heavy ions are cold particles, while the ions in the plasma sheet are significantly heated. In addition to its low temperature, the density compared to H^+ is rather small. Therefore, in this study, the heavy ions that diffuse directly from the cusp into the dayside cavity do not appear to significantly alter the magnetospheric dynamics.

4.2. The Role in Tail Stability

[43] Both simulations in this study show a reduced tail reconnection rate (or Earthward flow speed) after the mass loading in the magnetotail region. However, the magnetotail in the two simulations behave differently. A detailed examination of the magnetic field and mass density near the tail reconnection site reveals that the reduction of the reconnection rate is not simply associated with the increased mass density. In Figure 6, the magnetic field and mass density are obtained slightly above the equatorial tail X-line along the X-axis (i.e., midnight), with the position moving Earthward or tailward accordingly to the reconnection site. Indeed, the magnetic field around the reconnection site is clearly enhanced in the nightside auroal outflow simulation (Figure 6b), meaning that more magnetic flux actually flows into the X-line, assuming the size of the diffusion region does not change significantly. The enhancement in the magnetic field also appears in the first hour after the outflow initiation in the cusp outflow simulation (Figure 6a) before the stretching of the tail. Such an increase in the magnetic field shown in both simulations is evidently from the compression of the neutral sheet by the mass loading upon it.

[44] Nevertheless, during this period when magnetic energy is accumulated and stored in the tail (i.e., the growth phase if a substorm is going to occur), the tail responds differently in the two simulations. After the outflow begins, the nightside auroral outflow simulation shows a constantly steady tail with little change in the tail length through the entire simulation time, implying that the mass loading in the tail has little influence in initializing substorm onset, even though a growing amount of magnetic flux (Figure 6b) is advected into the reconnection region. In this sense, the ionospheric mass loading plays a negative role in the substorm occurrence. In other words, the ionospheric O^+ ions in the tail operate as an obstacle to slow down or postpone the substorm onset as opposed to the increased inflowing magnetic energy which is supposed to facilitate the substorm.

[45] However, the cusp outflow simulation indicates that the heavy ions in the tail help trigger the tail reconfiguration by first loading the mass source on to the plasma sheet, compressing the neutral sheet, accumulating magnetic energy in the tail and then disrupting the tail followed by another disruption.

[46] The different behavior of the tail in these two simulations strongly disagrees with previous assertions about the role of ionospheric heavy ions in the tail stability [e.g., *Nosé et al.*, 2009; *Baker et al.*, 1982]. The heavy ions appear not to play a definitive role of helping substorms to occur by disrupting the tail or to play a definitive role of preventing the substorms. Instead, the simulation study presented here shows that the influence of O^+ ions on the tail strongly depends on the origin of the ions and their corresponding pathways. Cusp-origin ionospheric outflow lands near the tail reconnection region, disturbing the magnetotail dramatically, while the nightside aurora-origin outflow plasma populates the near-Earth plasma sheet, preventing (or not encouraging) the release of the accumulated magnetic energy. Therefore, verifying the origin of the heavy ions before confirming their role in tail stability is necessary, rather than drawing any absolute conclusions.

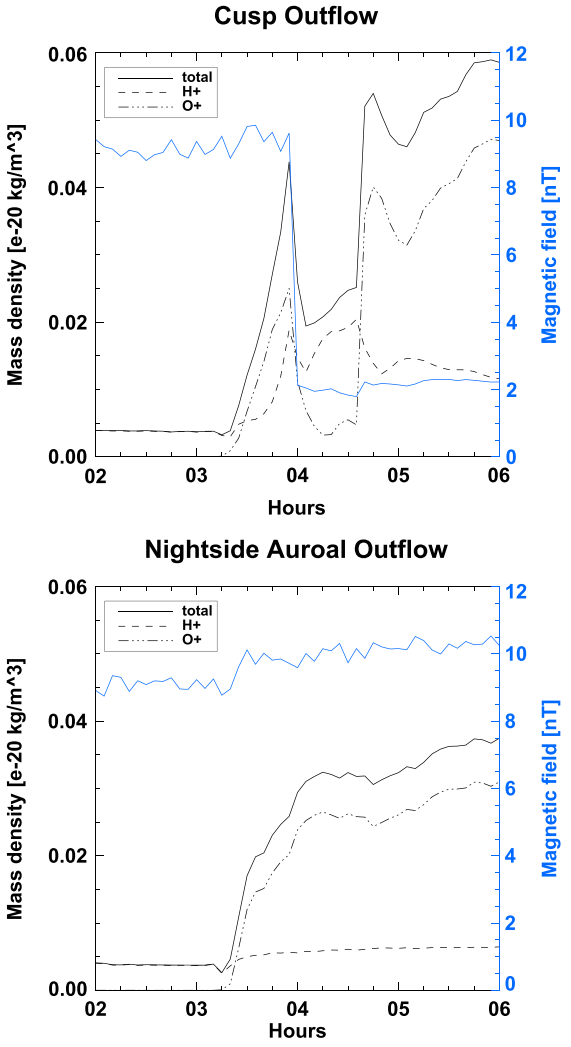

Figure 6. The mass density (black) and magnetic field (blue) slightly above the midnight tail reconnection site as a function of time in the cusp outflow simulation (upper) and nightside auroral outflow simulation (bottom).

[47] In actuality, it may not simply be the starting point (i.e., the source region) only that matters, but the starting point plus the ratio of the parallel and perpendicular velocities at the source, since this ratio determines where in the magnetosphere the O^+ will be deposited. A different outflow velocity near the Earth will result in a different landing

location with respect to the tail reconnection, feeding heavy ions to a different position in the tail. If this occurs, the tail dynamics may be quite different than the simulations presented here. In other words, altering the boundary conditions for the outflow is required to completely understand the origin-dependent role of the ionospheric outflow on the tail stability. This will be a future study.

4.3. Energization of Heavy Ions

[48] In the cusp outflow simulation, the specified O^+ outflow is at an energy of 100 eV; however, it takes them less than an hour to arrive at the near-Earth plasma sheet, less than the time described by *Fok et al*. [2006]. In the nightside auroral outflow simulation, the ionospheric heavy ions leak into the inner magnetosphere along the magnetic field lines in minutes. Even though a fast injection of ionospheric plasma is satisfied in the nightside auroral outflow simulation, there is still a lack of evidence that this rapid feeding of the plasma sheet is the reason for the intensified energy density in the inner magnetosphere, since the simulation results indicate that the direct outflow from the nightside auroral zone does not gain sufficient energy as needed.

[49] To analyze the energization along the trajectory of a particle flowing out of the ionospheric cusp, through the lobe, the central plasma sheet and then convecting to the nightside inner magnetosphere, a streamline of the heavy ions is followed at 06:00, as illustrated in Figure 7a. By 06:00, the particle flowline is relatively steady. Evidence of this can be observed by the stationary tail X-line (Figure 2b) and magnetopause (Figure 4) at the end of the simulation. On the other hand, the transport of the heavy ions from the inner boundary to the plasma sheet takes only tens of minutes (see Figure 1). Another concern is about the out-of-plane motion of the streamline as this particle flowline only considers the O^+ convection in the X-Z plane. Neglect of the out-of-plane motion is reasonable because the dominant flow is in the X-Z plane (Figure 7c) until the ions move away from the equator and along the magnetic field lines toward the Earth when the Y-component of the velocity becomes comparable to the X-component (indicated after the vertical line and the star marker in (a)). This part of the flowline will not be considered in the analysis.

[50] Figure 7b illustrates the energy density along the flowline at 06:00 of heavy ions. The energy density of heavy ions near the low altitude cusp region is high because of the high number density. During the flight from the high-altitude cusp through the lobes and close to the tail reconnection site, the energy density is very small. Following the encounter with the tail reconnection site, heating of the heavy ions is observed. This is the adiabatic energization when the particles move from the low- to high-magnitude magnetic field region. However, the adiabatic heating along the earthward convection does not fully account for the ring current energization, as the energy density is further enhanced by 130% near the outer boundary of the ring current (i.e., around -13 Re), due to the braking effect (note the sudden decrease in the velocity in Figure 7c) and the increase in density in the dipole region.

[51] The above results suggest that the ionospheric heavy ions in the plasma sheet are heated through adiabatic heating when they are transported from the tail reconnection site to the inner magnetosphere and subsequent localized energization

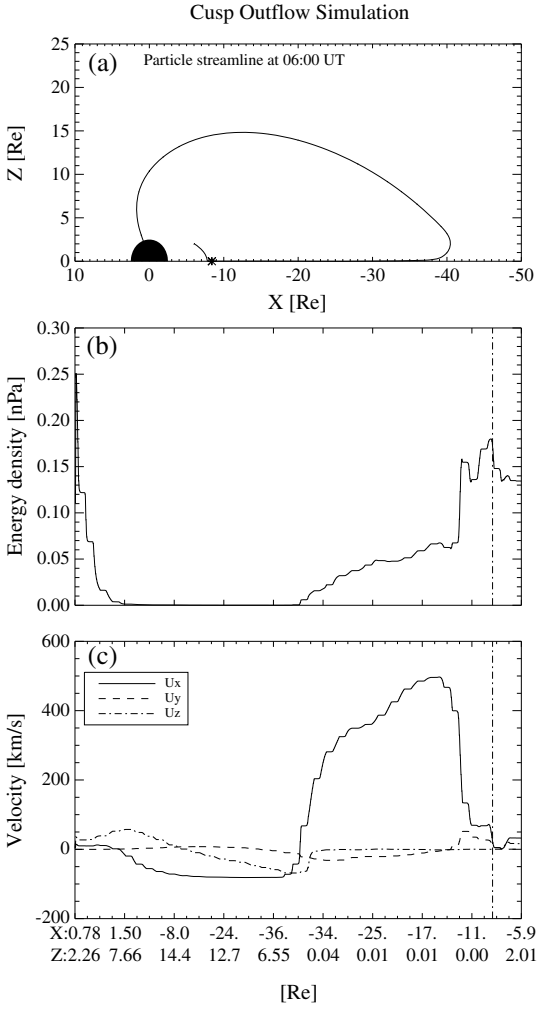

Figure 7. In the cusp outflow simulation, (a) a flowline of ionospheric cusp heavy ions at 06:00. (b) The energy density along this flowline. (c) The velocity along the streamline. The labels indicate the position of the flowline in the X-Z magnetosphere plane.

near the outer boundary of the ring current by flow braking (also adiabatic heating but due to flow convergence). While the flow-braking mechanism is not in the same category as localized nonadiabatic energization (the MHD simulation is unable to reveal kinetic dynamics) as suggested by early studies [*Nosé et al*., 2000b; *Delcourt*, 2002; *Fok et al*., 2006; *Nosé et al*., 2010], the idea of localized heating is consistent. In addition to the local energization, the "in-transit" adiabatic heating along the convective trajectory from the tail reconnection site to the inner region agrees with, for example, *Peroomian and El-Alaoui* [2008] and *Peterson et al*. [2009].

4.4. Ionosphere Feedback

[52] It should be noted again that these simulations are highly idealized. The outflow rate is held steady at the rates specified. In reality, as the energy into the ionosphere increases (through precipitation or Poynting flux), the outflow should increase, and vice versa. Studies such as that by *Brambles et al*. [2011] take into account such feedback into the ionosphere through the relationship between the Poynting flux and the outflow. Their results show periodic

dipolarization occurrence and thereby periodic enhanced energy inputs, which further periodically drives stronger ionospheric ions outflow and more mass loading into the magnetosphere. Such feedback is not taken into account in this study. The loading is persistently constant and eventually leads to a relatively steady configuration.

5. Conclusion

[53] Ionospheric outflow into the magnetosphere contributes an inertial interaction in the geospace system. How the ionospheric heavy ions load the magnetosphere and how that changes the magnetospheric dynamics are of great interest. In this study, two types of multifluid MHD simulations have been carried out: dayside cusp O^+ outflow and nightside auroral O^+ outflow. These are aimed at examining the impact of heavy ions originating from different source regions on the magnetospheric dynamics and exploring their energization as well as their role in influencing the tail stability. We have found the following results:

[54] 1. In contrast with the finding from many two-dimensional idealized multi-ion simulations regarding the role of heavy ions in reconnection [*Shay and Swisdak*, 2004], which found that the heavy ions increase the mass density near the reconnection site, reduce the Alfvén wave speed, and therefore decrease the reconnection rate, the presence of heavy ions in the magnetosphere does not translate to this simple scenario. Instead, the heavy ions can vary the topology and the state of the magnetosphere. The complicated dynamics subsequently leads to a change of the reconnection rate. Therefore, it is inappropriate to generally state that the increased amount of heavy ions in the magnetosphere leads to lower reconnection rates.

[55] 2. The local subsolar reconnection rate seems to decrease more when ionospheric heavy ions travel out from the dayside cusp region compared to when they travel out from the nightside aurora. This is associated with two factors: the attenuation of the magnetospheric field near the dayside magnetopause and the increase in the mass density near the subsolar magnetopause.

[56] 3. The total dayside reconnection rate is depressed more in the cusp outflow case, since the magnetopause moves inward due to the attenuated magnetospheric field, which is caused by the growth of the ring current and stronger tail current. While no significant change in the magnetospheric field or magnetopause position is observed in the nightside auroral outflow simulation, the total reconnection rate undergoes only a minor decrease.

[57] 4. The difference regarding the tail dynamics in these two simulations sheds some light on the argument about the role that heavy ions play in substorm occurrence. The role of heavy ions may have an origin dependence such that the cusp-origin heavy ions may facilitate substorms while nightside aurora-origin heavy ions probably hinder the substorm development or may not play a role in their occurrence.

[58] 5. The energization of heavy ions from the ionosphere into the ring current consists of two steps: an adiabatic heating after experiencing the tail reconnection and migrating toward the Earth and a localized heating by "flow braking" effect (i.e., adiabatic compressional heating) in front of the pressure wall near the outer boundary of the ring current.

Appendix A: Proof

[59] The following steps mathematically show that the total dayside reconnection rate is equivalent to the time change rate of the magnetic flux reconnected through the merging line. Assume the reconnection system has reached a steady state or varies slowly and the electric field is electrostatic, that is, $\mathbf{E} = -\triangle \Phi$. The potential drop along the merging line on the equatorial plane from dawn to dusk across the subsolar point) is then

$$\Delta\Phi = \int \mathbf{E}\cdot\mathbf{dl}. \tag{A1}$$

where $\mathbf{dl}$ is along the merging line on the magnetopause. After applying $\mathbf{E} = -\mathbf{v}\times\mathbf{B}$ (the resistivity term is negligible compared to the convection term according to *Hu et al*., [2009] to equation (A1), it becomes

$$\begin{aligned}\Delta\Phi &= -\int(\mathbf{v}\times\mathbf{B})\cdot\mathbf{dl}\\ &= \int\mathbf{B}\cdot(\mathbf{v}\times\mathbf{dl})\\ &= \int\mathbf{B}\cdot(\mathbf{v}dt\times\mathbf{dl})/dt\\ &= \int\mathbf{B}\cdot\mathbf{dS}/dt\\ &\simeq \frac{d\Phi_b}{dt}\end{aligned} \tag{A2}$$

where $\Phi_b = \int \mathbf{B}\cdot\mathbf{dS}$ is the magnetic flux flowing/reconnected through the boundary.

[60] **Acknowledgments.** The work at UM was supported by NSF ATM0639336, ANT0838828, and DoD FA95550-07-1-0434, and the work at LANL was supported by the U.S. Department of Energy through the Los Alamos National Laboratory/Laboratory Directed Research and Development (LDRD) program.

References

Baker, D. N., E. W. Hones, Jr., D. T. Young, and J. Birn (1982), The possible role of ionospheric oxygen in the initiation and development of plasma sheet instabilities, *Geophys. Res. Lett.*, *9*, 1337–1340, doi:10.1029/GL009i012p01337.

Borovsky, J. E., M. Hesse, J. Birn, and M. M. Kuznetsova (2008), What determines the reconnection rate at the dayside magnetosphere?, *J. Geophys.Res. (Space Physics)*, *113*, 7210, doi:10.1029/2007JA012645.

Brambles, O. J., W. Lotko, P. A. Damiano, B. Zhang, M. Wiltberger, and J. Lyon (2010), Effects of causally driven cusp O^+ outflow on the storm time magnetosphere-ionosphere system using a multifluid global simulation, *J. Geophys. Res.*, *115*, A00J04, doi:10.1029/2010JA015469.

Brambles, O. J., W. Lotko, B. Zhang, M. Wiltberger, J. Lyon, and R. J. Strangeway (2011), Magnetosphere Sawtooth Oscillations Induced by Ionospheric Outflow, *Sci.*, *332*, 1183–, doi:10.1126/science.1202869.

Cassak, P. A., and M. A. Shay (2007), Scaling of asymmetric magnetic reconnection: General theory and collisional simulations, *Phys. of Plasmas*, *14*(10), *102*,114, doi:10.1063/1.2795630.

Cully, C. M., E. F. Donovan, A. W. Yau, and G. G. Arkos (2003), Akebono/Suprathermal Mass Spectrometer observations of low-energy ion outflow: Dependence on magnetic activity and solar wind conditions, *J. Geophys. Res. (Space Phys.)*, *108*, 1093, doi:10.1029/2001JA009200.

Daglis, I. A., and W. I. Axford (1996), Fast ionospheric response to enhanced activity in geospace: Ion feeding of the inner magnetotail, *J. Geophys. Res. (Space Phys.)*, *101*, 5047–5066, doi:10.1029/95JA02592.

Daglis, I. A., and E. T. Sarris (1998), Comment on "Experimental investigation of possible geomagnetic feedback from energetic (0.1 to 16 keV) terrestrial O^+ ions in the magnetotail current sheet" by O. W. Lennartsson, D. M. Klumpar, E. G. Shelley and J. M. Quinn, *J. Geophys. Res.*, *103*, 29,545–29,548, doi:10.1029/98JA02268.

Delcourt, D. C. (2002), Particle acceleration by inductive electric fields in the inner magnetosphere, *J. Atmos. Sol.-Terr. Phys.*, *64*, 551–559, doi:10.1016/S1364-6826(02)00012-3.

Delcourt, D. C., C. R. Chappell, T. E. Moore, and J. H. Waite, Jr. (1989), A three-dimensional numerical model of ionospheric plasma in the magnetosphere, *J. Geophys. Res. (Space Phys.)*, *94*, 11,893–11,920, doi:10.1029/JA094iA09p11893.

Ebihara, Y., M. Yamada, S. Watanabe, and M. Ejiri (2006), Fate of outflowing suprathermal oxygen ions that originate in the polar ionosphere, *J. Geophys. Res.*, *111*, 4219, doi:10.1029/2005JA011403.

Elliott, H. A., J. Jahn, C. J. Pollock, T. E. Moore, and J. L. Horwitz (2007), O^+ transport across the polar cap, *J. Atmos. Sol.-Terr. Phys.*, *69*, 1541–1555, doi:10.1016/j.jastp.2007.06.003.

Fok, M., T. E. Moore, P. C. Brandt, D. C. Delcourt, S. P. Slinker, and J. A. Fedder (2006), Impulsive enhancements of oxygen ions during substorms, *J. Geophys. Res.*, *111*, 10,222, doi:10.1029/2006JA011839.

Gagne, J. (2005), Implementation of ionospheric outflow in the lfm global mhd magneto- spheric simulation, m.S. thesis, Dartmouth College.

Garcia, K. S., V. G. Merkin, and W. J. Hughes (2010), Effects of nightside O^+ outflow on magnetospheric dynamics: Results of multifluid MHD modeling, *J. Geophys. Res.*, *115*, A00J09, doi:10.1029/2010JA015730.

Glocer, A., G. Tóth, T. Gombosi, and D. Welling (2009a), Modeling ionospheric outflows and their impact on the magnetosphere, initial results, *J. Geophys. Res.*, *114*, 5216, doi:10.1029/2009JA014053.

Glocer, A., G. Tóth, Y. Ma, T. Gombosi, J. Zhang, and L. M. Kistler (2009b), Multifluid Block-Adaptive-Tree Solar wind Roe-type Upwind Scheme: Magnetospheric composition and dynamics during geomagnetic storms:Initial results, *J. Geophys. Res.*, *114*, 12,203, doi:10.1029/2009JA014418.

Hu, Y. Q., Z. Peng, C. Wang, and J. R. Kan (2009), Magnetic merging line and reconnection voltage versus IMF clock angle: Results from global MHD simulations, *J. Geophys. Res.*, *114*, 8220, doi:10.1029/2009JA014118.

Kistler, L. M., C. G. Mouikis, B. Klecker, and I. Dandouras (2010), Cusp as a source for oxygen in the plasma sheet during geomagnetic storms, *J. Geophys. Res.*, *115*, 3209, doi:10.1029/2009JA014838.

Kistler, L. M., et al. (2005), Contribution of nonadiabatic ions to the cross-tail current in an O^+ dominated thin current sheet, *J. Geophys. Res.*, *110*, 6213, doi:10.1029/2004JA010653.

Kistler, L. M., et al. (2006), Ion composition and pressure changes in storm time and nonstorm substorms in the vicinity of the near-Earth neutral line, *J. Geophys. Res.*, *111*, 11,222, doi:10.1029/2006JA011939.

Lennartsson, O. W., D. M. Klumpar, E. G. Shelley, and J. M. Quinn (1993), Experimental investigation of possible geomagnetic feedback from energetic (0.1 to 16 keV) terrestrial O(+) ions in the magnetotail current sheet, *J. Geophys. Res.*, *98*, 19,443, doi:10.1029/93JA01991.

Liao, J., L. M. Kistler, C. G. Mouikis, B. Klecker, I. Dandouras, and J.-C. Zhang (2010), Statistical study of o^+ transport from the cusp to the lobes with cluster codif data, *J. Geophys. Res.*, *115*, A00J15, doi:10.1029/2010JA015613.

Lockwood, M., J. H. Waite, Jr., T. E. Moore, C. R. Chappell, and M. O. Chandler (1985), The cleft ion fountain, *J. Geophys. Res.*, *90*, 9736–9748, doi:10.1029/JA090iA10p09736.

Lotko, W. (2007), The magnetosphere ionosphere system from the perspective of plasma circulation: A tutorial, *J. Atmos. Sol.-Terr. Phys.*, *69*, 191–211, doi:10.1016/j.jastp.2006.08.011.

Lyon, J., J. Fedder, and C. Mobarry (2004), The lyon-fedder-mobarry (lfm) global mhd magnetospheric simulation code, *J. Atmos. Sol.-Terr. Phys.*, *66*(1516), 1333–1350, doi:10.1016/j.jastp.2004.03.020, <ce:title>Towards an Integrated Model of the Space Weather System</ce:title>.

Moore, T. E., M. Fok, S. P. Christon, S. Chen, M. O. Chandler, D. C. Delcourt, J. Fedder, S. Slinker, and M. Liemohn (2005), Solar and Ionospheric Plasmas in the Ring Current Region, *Washington DC Am. Geophys. Union Geophys. Monogr. Ser.*, *159*, 179.

Moore, T. E., M. Fok, D. C. Delcourt, S. P. Slinker, and J. A. Fedder (2010), Global response to local ionospheric mass ejection, *J. Geophys. Res.*, *115*, A00J14, doi:10.1029/2010JA015640.

Nosé, M., A. T. Y. Lui, S. Ohtani, B. H. Mauk, R. W. McEntire, D. J. Williams, T. Mukai, and K. Yumoto (2000a), Acceleration of oxygen ions of ionospheric origin in the near-Earth magnetotail during substorms, *J. Geophys. Res.*, *105*, 7669–7678, doi:10.1029/1999JA000318.

Nosé, M., S. Ohtani, A. T. Y. Lui, S. P. Christon, R. W. McEntire, D. J. Williams, T. Mukai, Y. Saito, and K. Yumoto (2000b), Change of energetic ion composition in the plasma sheet during substorms, *J. Geophys. Res.*, *105*, 23,277–23,286, doi:10.1029/2000JA000129.

Nosé, M., S. Taguchi, K. Hosokawa, S. P. Christon, R. W. McEntire, T. E. Moore, and M. R. Collier (2005), Overwhelming O^+ contribution to the plasma sheet energy density during the October 2003 superstorm: Geotail/EPIC and IMAGE/LENA observations, *J. Geophys. Res.*, *110*, 9, doi:10.1029/2004JA010930.

Nosé, M., A. Ieda, and S. P. Christon (2009), Geotail observations of plasma sheet ion composition over 16 years: On variations of average plasma ion mass and O^+ triggering substorm model, *J. Geophys. Res.*, *114*, 7223, doi:10.1029/2009JA014203.

Nosé, M., H. Koshiishi, H. Matsumoto, P. C:son Brandt, K. Keika, K. Koga, T. Goka, and T. Obara (2010), Magnetic field dipolarization in the deep inner magnetosphere and its role in development of O^+ -rich ring current, *J. Geophys. Res.*, *115*, A00J03, doi:10.1029/2010JA015321.

Peroomian, V., and M. El-Alaoui (2008), The storm-time access of solar wind ions to the nightside ring current and plasma sheet, *J. Geophys. Res.*, *113*, 6215, doi:10.1029/2007JA012872.

Peroomian, V., M. El-Alaoui, M. A. Abdalla, and L. M. Zelenyi (2006), Dynamics of ionospheric O^+ ions in the magnetosphere during the 24-25 September 1998 magnetic storm, *J. Geophys. Res.*, *111*, 12,203, doi:10.1029/2006JA011790.

Peterson, W. K., H. L. Collin, O. W. Lennartsson, and A. W. Yau (2006), Quiet time solar illumination effects on the fluxes and characteristic energies of ionospheric outflow, *J. Geophys. Res.*, *111*, 11, doi:10.1029/2005JA011596.

Peterson, W. K., L. Andersson, B. Callahan, S. R. Elkington, R. W. Winglee, J. D. Scudder, and H. L. Collin (2009), Geomagnetic activity dependence of O^+ in transit from the ionosphere, *J. Atmos. Sol.-Terr. Phys.*, *71*, 1623–1629, doi:10.1016/j.jastp.2008.11.003.

Ridley, A. J., T. I. Gombosi, and D. L. D. Zeeuw (2004), Ionospheric control of the magnetospheric configuration: Conductance, *Ann. Geophys.*, *22*, 567.

Ridley, A. J., D. L. de Zeeuw, W. B. Manchester, and K. C. Hansen (2006), The magnetospheric and ionospheric response to a very strong interplanetary shock and coronal mass ejection, *Adv. Space Res.*, *38*, 263–272, doi:10.1016/j.asr.2006.06.010.

Ridley, A. J., T. I. Gombosi, I. V. Sokolov, G. Tóth, and D. T. Welling (2010), Numerical considerations in simulating the global magnetosphere, *Ann. Geophys.*, *28*, 1589–1614, doi:10.5194/angeo-28-1589-2010.

Shay, M. A., and M. Swisdak (2004), Three-species collisionless reconnection: Effect of o^+ on magnetotail reconnection, *Phys. Rev. Lett.*, *93*, 175,001, doi:10.1103/PhysRevLett.93.175001.

Sheldon, R. B., H. E. Spence, and J. F. Fennell (1998), Observation of the 40 keV field-aligned ion beams, *grl*, *25*, 1617–1620, doi:10.1029/98GL01054.

Strangeway, R. J., R. E. Ergun, Y. Su, C. W. Carlson, and R. C. Elphic (2005), Factors controlling ionospheric outflows as observed at intermediate altitudes, *J. Geophys. Res.*, *110*, 3221, doi:10.1029/2004JA010829.

Tóth, G., et al. (2005), Space Weather Modeling Framework: A new tool for the space science community, *J. Geophys. Res.*, *110*, 12,226, doi:10.1029/2005JA011126.

Tung, Y., C. W. Carlson, J. P. McFadden, D. M. Klumpar, G. K. Parks, W. J. Peria, and K. Liou (2001), Auroral polar cap boundary ion conic outflow observed on FAST, *J. Geophys. Res.*, *106*, 3603–3614, doi:10.1029/2000JA900115.

Wang, H., A. J. Ridley, and H. Lühr (2008), Validation of the Space Weather Modeling Framework using observations from CHAMP and DMSP, *Space Weather*, *6*, S03001, doi:10.1029/2007SW000355.

Welling, D. T., and A. J. Ridley (2010), Validation of SWMF magnetic field and plasma, *Space Weather*, *8*, S03002, doi:10.1029/2009SW000494.

Wiltberger, M., W. Lotko, J. G. Lyon, P. Damiano, and V. Merkin (2010), Influence of cusp O^+ outflow on magnetotail dynamics in a multifluid MHD model of the magnetosphere, *J. Geophys. Res.*, *115*, A00J05, doi:10.1029/2010JA015579.

Winglee, R. M. (2003), Circulation of ionospheric and solar wind particle populations during extended southward interplanetary magnetic field, *J. Geophys. Res.*, *108*, 1385, doi:10.1029/2002JA009819.

Winglee, R. M., D. Chua, M. Brittnacher, G. K. Parks, and G. Lu (2002), Global impact of ionospheric outflows on the dynamics of the magnetosphere and cross-polar cap potential, *J. Geophys. Res.*, *107*, 1237, doi:10.1029/2001JA000214.

Yau, A. W., and M. André (1997), Sources of ion outflow in the high latitude ionosphere, *Space Sci. Rev.*, *80*, 1.

Yu, Y., and A. J. Ridley (2008), Validation of the space weather modeling framework using ground-based magnetometers, *Space Weather*, *6*, S05002, doi:10.1029/2007SW000345.

Yu, Y., and A. J. Ridley (2009a), Response of the magnetosphere-ionosphere system to a sudden southward turning of interplanetary magnetic field, *J. Geophys. Res.*, *114*, A03216, doi:10.1029/2008JA013292.

Yu, Y., and A. J. Ridley (2009b), The response of the magnetosphere-ionosphere system to a sudden dynamic pressure enhancement under southward IMF conditions, *Ann. Geophy.*, *27*, 4391–4407, doi:10.5194/angeo-27-4391-2009.

Yu, Y., A. J. Ridley, D. T. Welling, and G. Tóth (2010), Including gap region field-aligned currents and magnetospheric currents in the MHD calculation of ground-based magnetic field perturbations, *J. Geophys. Res.*, *115*, A08207, doi:10.1029/2009JA014869.